Int. J. Electrochem. Sci., 10 **(2015)** 5812 - 5826

International Journal of
ELECTROCHEMICAL
SCIENCE
www.electrochemsci.org

Influence of Green Corrosion Inhibitor based on Chitosan Ionic Liquid on the Steel Corrodibility in Chloride Solution

Gamal A. El-Mahdy[1,2], Ayman M. Atta[1,3], Hamad A. Al-Lohedan[1] and Abdelrahman O. Ezzat[1]*

[1]Surfactants research chair, Department of Chemistry, College of Science, King Saud University, P.O.Box 2455, Riyadh 11451, Saudi Arabia
[2] Chemistry department, Faculty of Science, Helwan University, Helwan 11795, Egypt
[3] Petroleum application department, Egyptian petroleum research institute, Nasr city 11727, Cairo, Egypt.
[*]E-mail: khaled_00atta@yahoo.com

Received: 18 April 2015 / *Accepted:* 11 May 2015 / *Published:* 27 May 2015

Ionic liquids (ILs) attracted great attention as green corrosion inhibitors for steel in aggressive environments. The present work synthesize new IL using chitosan through amidation and quaternization reaction with oleic acid and p-toluene sulfonic acid, respectively. The chemical structure of the prepared polymeric ionic liquid was investigated using NMR analysis. The corrosion inhibitive effect of the prepared polymeric ionic liquid on steel corrosion in acid chloride solution was studied using different electrochemical techniques. Potentiodynamic polarization data revealed that the prepared ionic liquid reduces both dissolution and hydrogen evolution corrosion reactions. Impedance technique shows one capacitive loop that indicated the charge-transfer process of the steel corrosion. Langmuir isotherms found to fit properly the adsorption of the prepared polymeric ionic liquid over the steel surfaces.

Keywords: corrosion inhibition, Polarization, EIS, Acid medium, adsorption

1. INTRODUCTION

Green organic corrosion inhibitors based on natural materials attracted more attentions last decades and replaced the inhibitors based on toxic materials produced from petrochemical resources [1, 2]. Ionic liquids (ILs) have an promise future in the field of green chemistry due to their utilization will effectively reduce the risk of environment. The ILs (organic salts) become the most widely inhibitors used in the petroleum fields due to their negligible vapor pressure, high thermal stability, low melting below 100 ^{o}C, low glass transition temperature, low toxicity, high surface activities and

high sensitivity to salts [3-5]. These materials showed high performance to adhere on the surface of steel with the formation of thin films to protect the steel, copper and aluminum substrates [6-9]. Moreover, the high vapor pressure , high ionic conductivity, and non-flammability of ionic liquids, ILs, increased their applicability in the petroleum fields to protect petroleum pipe-lines and equipments from acids and salts corrosions. There are several studies used ILs to protect the petroleum equipments from CO_2 and H_2S corrosions [10, 11].

The chitosan polymeric forms based on amino-polysaccharides produced several new materials due to high ability for functionalization to apply in several industrial applications because of their better solubility in organic solvents and water than chitosan itself [12-15]. Nowadays, the chitosan derivatives possess unique properties become the most applicable research area such as water treatments, agriculture and medical industry [16-20]. ILs are one of the most applicable materials that were produced from chitosan polymers [21, 22]. Although ILs do not evaporate and will not pollute the environment but there are some famous ILs for example, [PF6] and [BF4] organic salts decomposed in wwater to produce harmful products such as hydrofluoric and phosphoric acids which are hazard to the environment [23]. The objective of the present work is to prepare new IL based on chitosan through amidation and quaternization reaction with oleic acid and p-toluene sulfonic acid, respectively. Moreover, the ability of the prepared materials to inhibit the corrosion of steel in 1 M solution of HCl was investigated by different electrochemical techniques. The steel surface morphology was scanned to detect the performance of the films formed by applying the IL at different concentrations in acid solution using Scanning electron microscopy (SEM).

2. EXPERIMENTAL

2.1. Materials

Chitosan of 100mesh has molecular weight 77 KDa, was extracted from crab shell, 1-ethyl-3-(3-dimethylaminopropyl) carbodiimide hydrochloride (EDC), oleic acid (OA) and p-toluene sulfonic acid monohydrate (PTSA; 99.5%) were obtained from Aldrich Chemicals Co. Acid chloride (37 wt%) was obtained from Merck Co. Distilled water was used for preparing test solutions for all measurements. The chemical composition, the method of electrode preparation of the working electrode, the reference and the counter electrode are the same as used previously in our studies [24]

2.2. Synthesis procedure

a) Synthesis of chitosan-p-toluene sulfonate salt (CSPTA)

PTSA (4.75 g; 0.025 mol) was added in 100 mL distilled water and equal mol amounts of Cs (3.75 g; 0.025 mol) were mixed with stirring in nitrogen atmosphere in a flask equipped with thermometer and reflux condenser. The reaction temperature was increased to 70 ^{o}C and maintained for 24 h. Finally, the reaction mixture was poured in acetone and washed with diethylether to remove

the unreacted materials. The precipitate was dried in vacuum oven at 45 ^{o}C. The product of reaction yield was 70 % and designated as CSPTA.

b) Amidation of CPSTA with OA

CSPTA (2 g) was solubilized in water 100 mL. OA(1.27 g) was mixed with methanol (85 mL) and added dropwise to the reaction with stirring. The mol ratio between OA and CSPTA solution is 0.34 mol/mol glucosamine residue. EDC (15 mL) dissolved in methanol (0.07 g/L) was added dropwise at room temperature. The mole ratio of OA to DEC is 1. The reaction is completed under stirring in nitrogen atmosphere for 24 hrs. The reaction mixture poured into 200 mL acetone to isolate the product. The precipitate was filtered, washed with distilled methanol, ether, and dried under vacuum at 20 °C. The amidated CSPTA was designated as CSPTA-OA.

2.3. Characterization

^{1}H- and ^{13}CNMR spectra of the prepared ionic liquids were recorded on a 400MHz Bruker Avance DRX-400 spectrometer.

The surface tension measurements of IL solutions and contact angles between aqueous acid solution were measured using drop shape analyzer model DSA-100.

2.4 Electrochemical measurements

Electrochemical measurements were performed using the Solartron 1470E (multichannel system) as electrochemical interface and the Solartron 1455A as FRA. The potentiodynamic polarization measurement was at a sweep rate of 1 mV/s. EIS measurements were carried out over a frequency range of 10 kHz–10 mHz.

3. RESULTS AND DISCUSSION

It was previously reported that the presence of intra- and intermolecular hydrogen bonds have a significant effects to decrease the solubility of chitosan in aqueous medium [25]. The solubility of chitosan in aqueous basic solution was occurred by using urea and guanidine hydrochloride through deprotonation of amino group in chitosan. Moreover, there are several routes used to modify the solubility of chitosan in water through introducing the hydrophilic groups such as quaternization, carboxymethylation and grafting with poly(ethylene glycol) [26-31]. In this respect, the present work aims to change the solubility of Cs in water by quaternization 60% of Cs amine group with PTSA. Moreover, the quaternized product was amidated with oleic acid in the presence of EDC as catalyst to produce amphiphilic ionic liquid based on Cs. The reaction scheme represents in the Scheme 1.

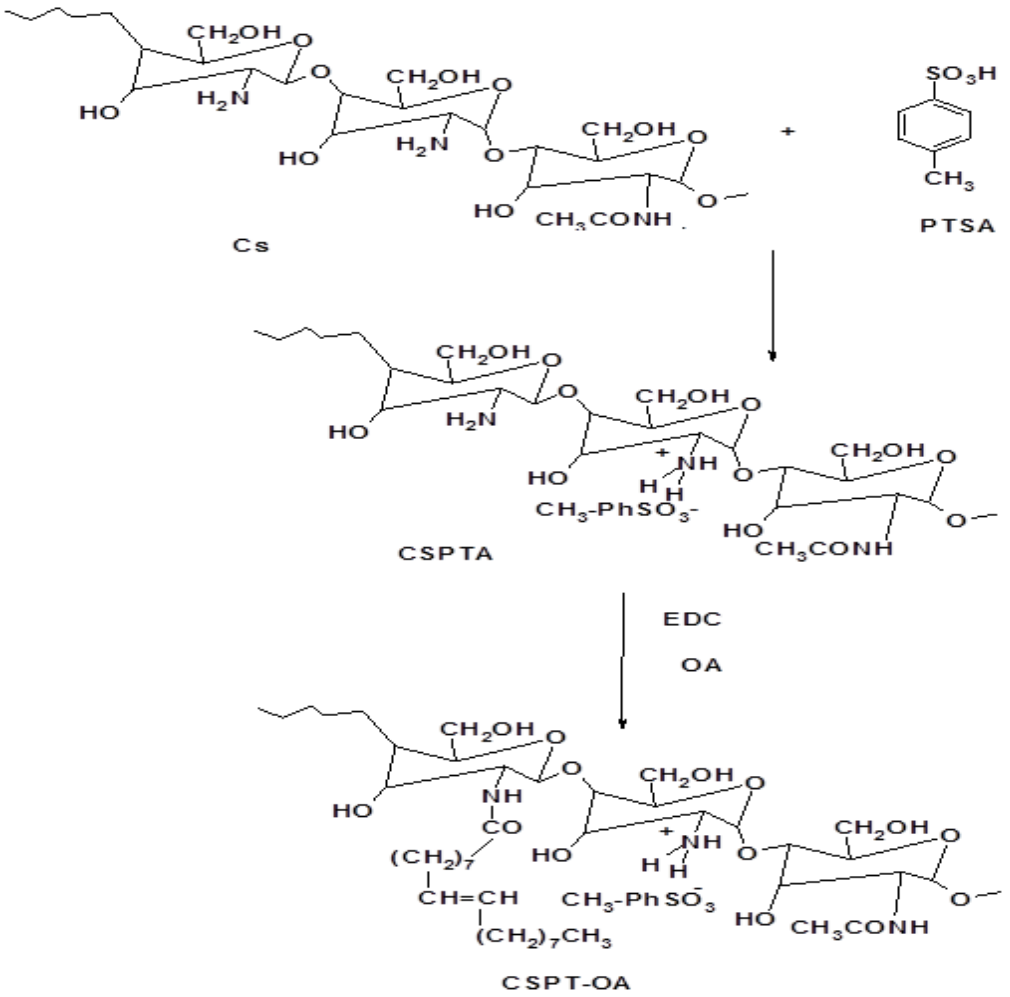

Scheme 1. Synthesis of CSPTA-OA.

3.1. Chemical structure of amphiphilic chitosan

The chemical structures of the produced CSPTA and CSPTA-OA are elucidated using FTIR and NMR analyses. In this respect, their FTIR and ^{1}HNMR spectra are illustrated in Figures 1 and 2, respectively. Formation of quaternized CS-PTS was confirmed by FTIR spectroscopy (Figure 1a), which shows bands at 3100 and 980 cm^{-1} assigned for CH stretching and out –of-plan bending of phenyl group of PTSA. The characteristic broad—OH band of CS is observed at 3450 cm^{-1}. The appearance of band at 1040 cm^{-1}, which attributed to S=O stretching frequency of PTSA indicates the formation of quaternized CSPTA. The spectrum of amidated CSPTA-OA, Figure 1b, shows three new absorption bands at 1700, 1650 and 1500 cm^{-1}, which are attributed to the inter-, intra- and non-bonded amide—NH groups, respectively [32].

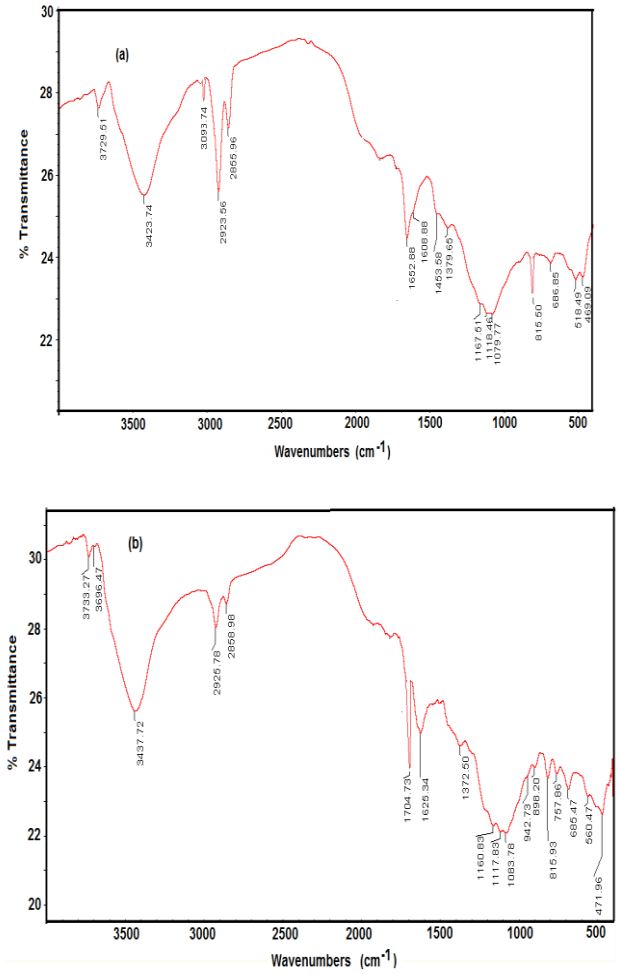

Figure 1. FTIR spectra of a) CSPTA and b) CSPTA-OA.

The ^{1}HNMR spectra of CSPTA and CSPTA-OA are illustrated in Figure 2a and b, respectively, and used to confirm their chemical structure as represented in the scheme 1. Figure 2 shows peaks at chemical shifts (δ) 7.709 ppm (doublet, 2H, J = 8.1 Hz), and 7.24 ppm (doublet of doublet, 2H, J = 8.4, 0.6 Hz, HW) represent phenyl protons indicated the incorporation of PTSA as anion in the chemical structures of CSPTA and CSPTA-OA. Moreover, the appearance of broad peaks at 8.5 ppm represents $^{+}NH_3$- and confirms the quaternization of amino groups of CS. The amidation of OA with CSPTA can be confirmed by appearance on new peaks at 0.83 (triplet), 1.5 (multiple) and 5.3 ppm (multiple) that assign for CH_3, $(CH_2)_7$ and –CH=CH-, of OA respectively. The peak at δ 3.2 ppm confirms the methylene group (CH_2-OH) of CS. The disappearance of peaks at 2.9ppm (2 H) is attributed to C-NH_2 (CS) indicates that there is no any free amine groups in CS after quaternization and amidation with PTSA and OA, respectively. ^{1}HNMR analysis can be used here to determine the degree of CS amidation with OA and quaternization by comparing the integrations of peaks at δ = 8.5 ($^{+}NH_3$-) and 0.83 ppm (CH_3, oleic). The peak integrations indicate that the ratio between quaternization and amidation was 2: 1 which confirms that 60 and 30 mol % of amine groups are quaternized and amidated, respectively. These data agree with mol % of added PTSA and OA to CS as explained in the experimental section.

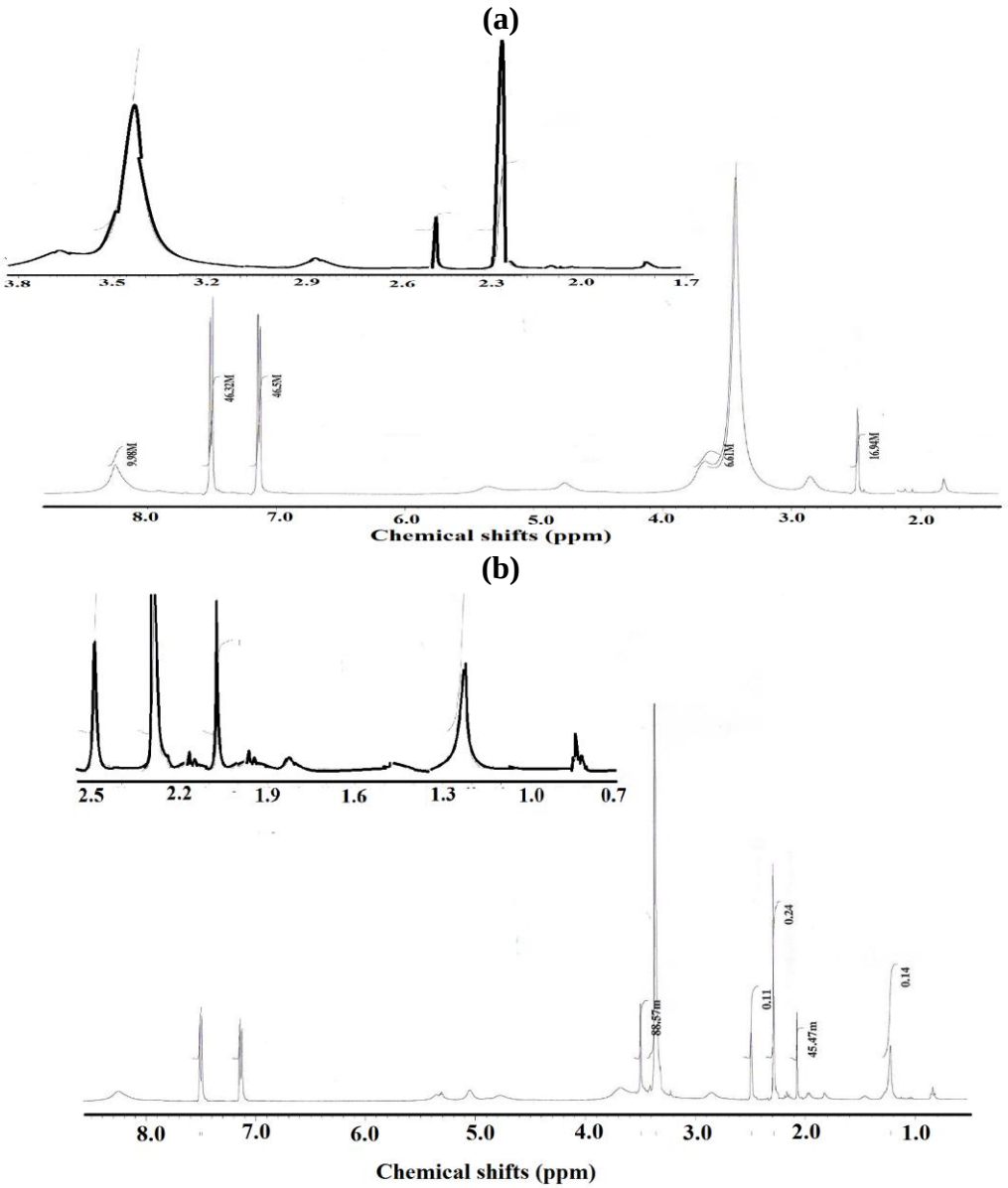

Figure 2. ^{1}HNMR spectra of a) CSPTA and b) CSPTA-OA.

3.2. Surface Activity of amphiphilic chitosan

The molecular structure of CSPTA and CSPTA-OA indicates that there are differences between hydrophilicity and hydrophobicity of the prepared compounds when compared to CS. These differences will reflect on the interaction between the modified CS products with water and acid solution (1 M HCl). It is expected that CSPTA and CSPTA-OA possess different surface activity properties. In this respect, the adsorption isotherms of CSPTA and CSPTA-OA are used to determine the surface activity parameters such as the effectiveness of the surface tension reduction (π_{cmc}), the concentration of surfactants at the water-air interface Γ_{max} and the area per molecule $A_{min.}$at the interface. The adsorption isotherm plots (relations between surface tension (γ, mN/m) and their

concentrations ln c (mol/L) are measured in water and 1M HCl at 25 ^{o}C and plotted in Figure 3. The CSPTA shows constant γ that reduces from 72.1 to 52.3 mN/m at CSPTA concentration 5 x 10^{-3} mol/L and temperature 25 ^{o}C. These data indicate the presence of quaternary amine salt and absence of any hydrophobic groups in CS affects the adsorption of CSPTA at air/water interface and increased their interaction in the bulk solution [33, 34]. This characteristic indicates that CSPTA behaves as polyelectrolyte in water solution. The data of surface activity of CSPTA-OA in water and 1 M HCl are calculated and tabulated in Table 1.

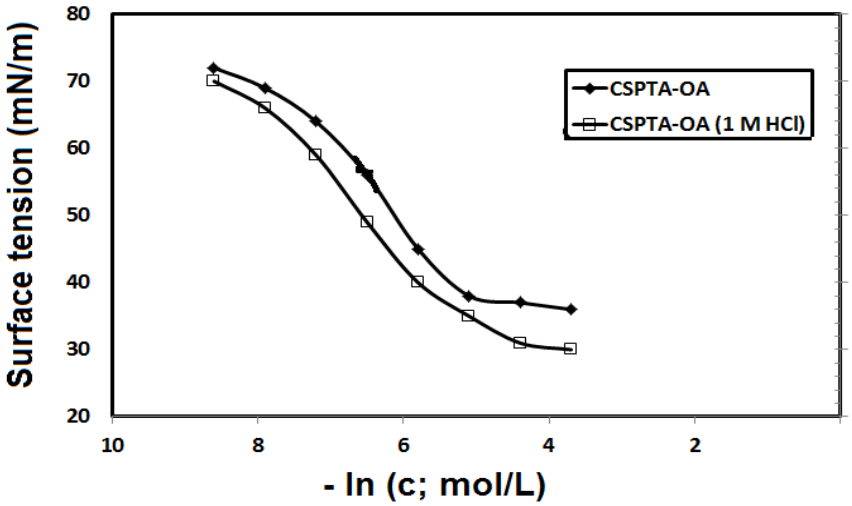

Figure 3. Adsorption isotherms of CPTA -OA in water and 1M HCl solution at 25 ^{o}C.

Table 1. Surface activity parameters of amphiphile chitosan in water and 1M HCl solution at 25 ^{o}C.

Designation	cmc mol/L x 10^{3}	γ_{cmc} mN/m	π_{cmc} mN/m	$(-\partial \gamma / \partial \ln c)$	Γ_{max} x 10^{10} mol/ cm^{2}	A_{min} nm^{2}/ molecule
CSPTA-OA In water	6.1	37.1	47.1	11.2	4.50	0.41
CSPTA-OA In 1M HCl	6.1	31.1	41.1	14.1	5.89	0.28

The critical micelle concentration (cmc, mol/L) of CSPTA-OA surfactant in 1M HCl and water does not change but the surface tension at cmc (γ_{cmc}) was increased from 31.6 to 37.2 mN/m in 1M HCl and water, respectively. The effectiveness π_{cmc}, which determined from relation; $\pi_{cmc} = \gamma_o - \gamma_{cmc}$; where γ_o is the surface tension of water without surfactants(72.1 mN/m at 25 ^{o}C), is increased in 1M HCl due to greater reduction of surface tension in 1M HCl. These data indicate that possesses high surface activity in 1M HCl. This result demonstrates that the presence of high percentages of hydrophobic substituent (oleic group) in the chemical structure of CSPTA-OA increases its amphiphilic characteristic. The value of $\Gamma_{max.}$ (mol/cm^{2}) of CSPTA-OA in 1M HCl and water, are calculated from equation: $\Gamma_{max.} = - [(\delta \gamma / \delta \ln c)/RT]$, where $(\delta \gamma / \delta \ln c)$ is the slope of the plot of c

versus ln c. Careful inspection of Γ_{max} values indicate that the quantity of the CSPTA-OA surfactant adsorb more at air/water interface in 1M HCl. Moreover, the minimum area per molecule $A_{min.}$ (nm^2 / mol) at the aqueous-air interface, calculated using the equation: $A_{min.} = 10^{16} / \Gamma_{max} N$; where N is Avogadro's number, is reduced in the presence of 1M HCl. The lowest value of A_{min} suggests that the adsorption of CSPTA-OA which oriented away from the liquid in a more tilted position in 1M HCl. However, a low A_{min} data suggest complete surface coverage with the formation of flexible CSPTA-OA chains at interface in 1 M HCl.

3.3 Potentiodynamic polarization measurements

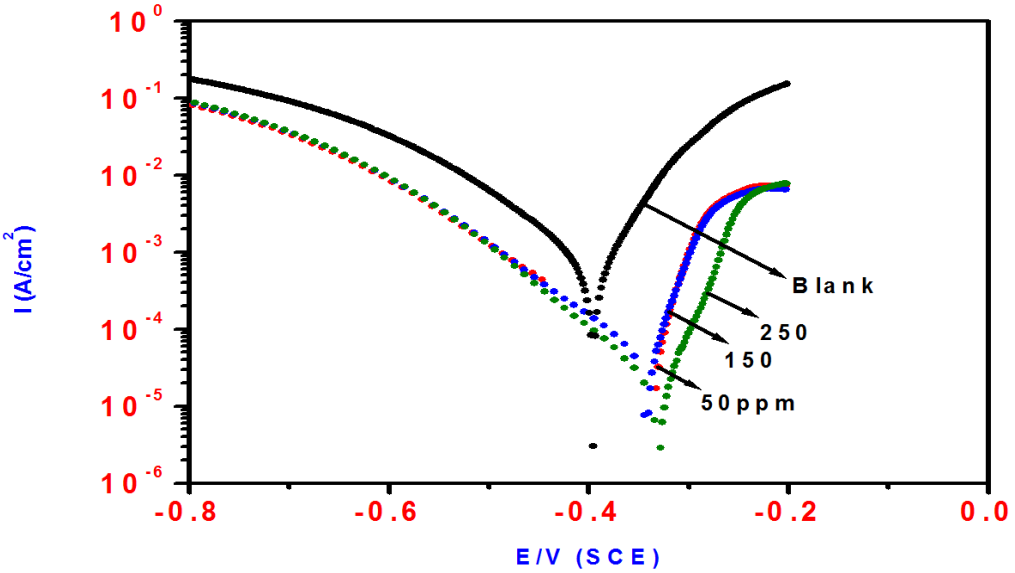

Figure 3. The effect of CSPTA concentrations on the polarization curves of steel in acidic chloride solutions.

The current–potential relationship without and with different concentrations of CSPTA and CSPTA-OA is depicted in Figures 4 and 5, respectively. The inhibited solution containing CSPTA and CSPTA-OA showed a pronounced an ennoblement in the in the values of Ecorr in the anodic direction . It is clear that the additions of both inhibitors are accompanied by lowering the corrosion current density than that of experienced by the blank solution. The data presented in Figures 4 and 5 indicated the formation of inhibitive film, which blocked the active sites on the steel surface and retarded the diffusion of corrosive ions to the steel substrate. This data confirms that that the inhibitor strongly suppressed the corrosion process of steel . Hence, both inhibitors behaved as mixed-type inhibitor by reducing both the cathodic and anodic reactions [35-36]

All the values of the estimated electrochemical parameters are quoted in Tables 2 and 3 for CSPTA and CSPTA-OA, respectively. The inhibition efficiency was estimated using the relation[37-39]:

$$IE(\%) = 1- (i_{inhibited} / i_{uninhibited}) \times 100 \quad (1)$$

where $i_{nhibited}$ and $i_{uninhibited}$ are the inhibited and uninhibited corrosion current densities, respectively.

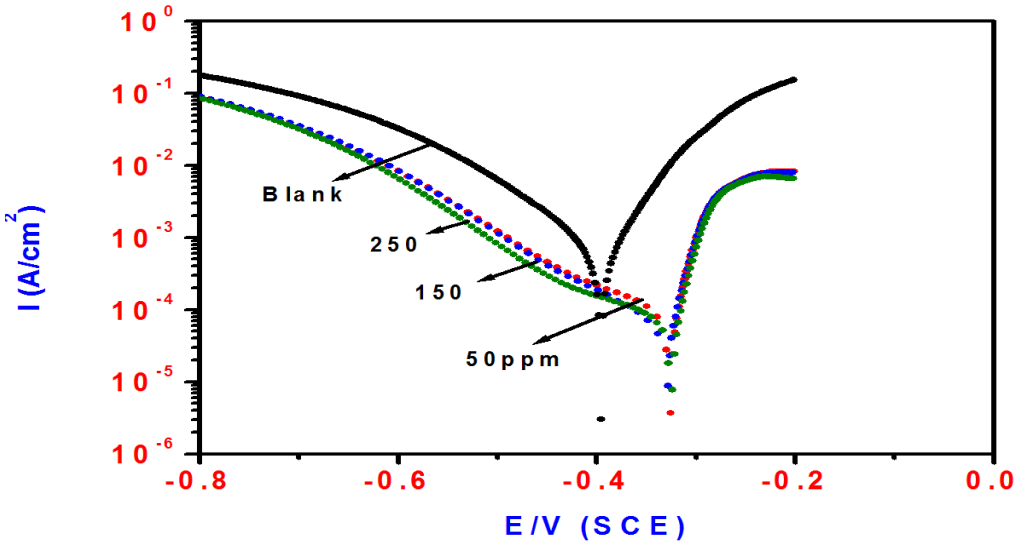

Figure 4. The effect of CSPTA-OA concentrations on the polarization curves of steel in acidic chloride solutions.

The calculated values of IE% are shown in Tables 2 and 3 for CSPTA and CSPTA-OA, respectively. The high inhibition efficiency experienced with increasing the inhibitor concentration could be attributed to a reduction in corrosion current density. The results can explained on the basis of adsorption of both inhibitors on the steel surface and the amount of adsorbed inhibitor increased with increasing the concentration. Data in the Tables 2 and 3 show that the addition of CSPTA and CSPTA-OA to the blank solution is accompanied by a shift in Ecorr to the noble direction with a more pronounced increasing in the inhibition efficiency with increasing inhibitor concentration. This result can be attributed a reduction in the corrosion current densities (icorr). In addition, CSPTA has more corrosion protection performance than that experienced with CSPTA-OA.

Table 2. The effect of **CSPTA** concentrations on the IE% values for steel in acidic chloride solutions using electrochemical methods.

	Polarization Method					EIS Method		
	Ba (mV)	Bc (mV)	E_{corr} (V)	i_{corr} $\mu A/cm^2$	IE%	R_{ct} Ohm	Cdl ($\mu F/cm^2$)	IE%
Blank	69	120	-0.3955	839	_____	1.80	334	____
50ppm	62	163	-0.3357	95	88.6	16.5	112	89.1
150	56	103	-0.3425	39	95.3	40	103	95.5
250	44	94	-0.3302	19	97.7	83	93	97.8

Table 3. The effect of **CSPTA-OA** concentrations on the IE% values for steel in acidic chloride solutions using electrochemical methods.

	Polarization Method					EIS Method		
	Ba (mV)	Bc (mV)	E_{corr} (V)	i_{corr} $\mu A/cm^2$	IE%	R_{ct} Ohm	Cdl ($\mu F/cm^2$)	IE%
Blank	69	120	-0.3955	839	_____	1.80	334	____
50ppm	57	178	-0.3269	96	88.5	16	115	88.7
150	58	180	-0.3317	88	89.5	18	107	90
250	53	124	-0.3328	35	95.4	41	101	95.6

3.4. Electrochemical Impedance Spectroscopy studies

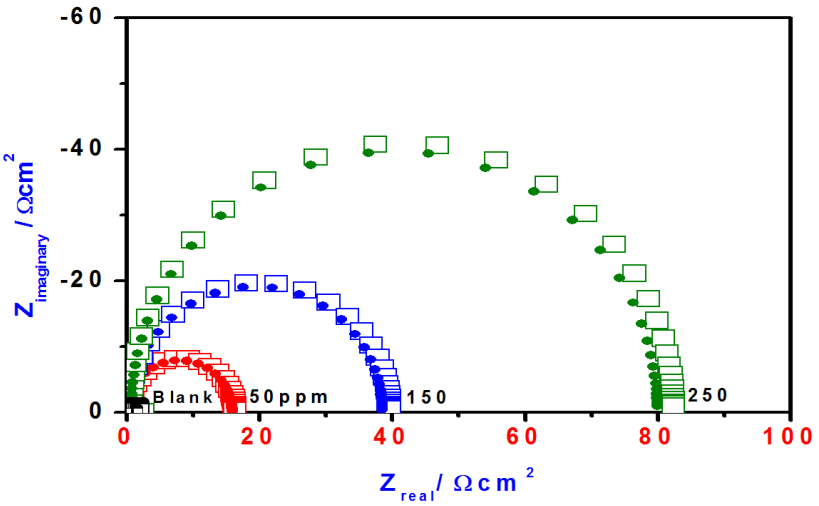

Figure 6. The effect of CSPTA concentrations on the Nyquist plot of steel in acidic chloride solutions.

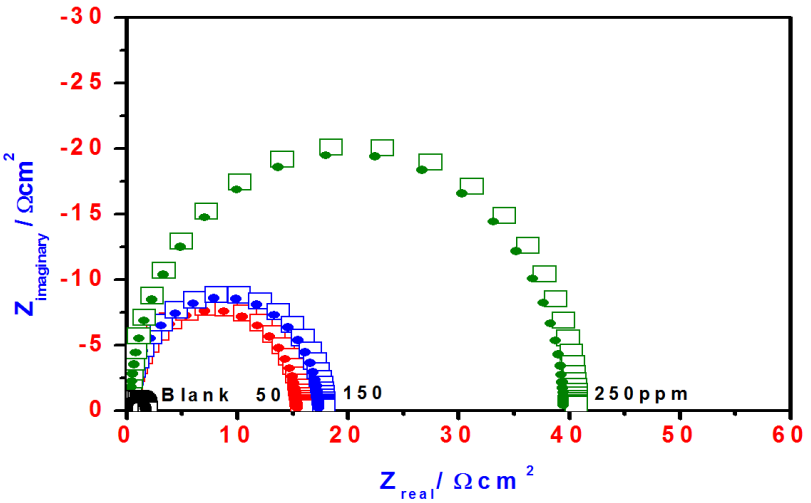

Figure 7. The effect of CSPTA-OA concentrations on the Nyquist plot of steel in acidic chloride solutions.

The corrosion inhibition behavior of steel in 1 M HCl in the absence and presence of different concentrations of CSPTA and CSPTA-OA can be also investigated using EIS technique Figures 6 and 7 depict the Nyquist plots obtained from impedance data without and with different concentrations of CSPTA and CSPTA-OA, respectively. Figures 6 and 7 show the formation of one capacitive loop in the Nyquist plot. The corrosion phenomenon is usually associated with the double-layer behavior[40]. The diameter of the capacitive loop becomes more larger in the presence of inhibitor and increases with the concentration of the inhibitor. The capacitive loop indicated that the corrosion of steel is mainly controlled by a charge-transfer reaction [41-42]. The data shown in Figures 6-7 were fitted by circuit composed of (Rs), (Cdl) and (Rct)

The estimated values of Rct and Cdl derived from Nquist plots in the absence and presence of different concentrations of CSPTA and CSPTA-OA are given in Tables 2 and 3, respectively. Data in the Tables 2 and 3 clearly show that the values of Cdl decreased, while the values of Rct increased in the presence of both inhibitor and is highly dependent upon inhibitor concentration. The increase in Rct values in the inhibited solutions along with the diameter of the capacitive loop , confirms the corrosion protection efficiency of CSPTA and CSPTA-OA. The adsorbed inhibitor layer on steel surface reduced the stored electric charge, which acts as dielectric constant. Increasing the thickness of the adsorbed layer led to an increase in the value of Cdl.

The result indicates that both inhibitor act as inhibitors, by adsorption via replacing the adsorbed water molecules at the steel–solution interface[43]. The inhibition efficiency can be calculated from the results obtained by using the following equation [44-46]:

$$IE\% = 1 - (R^1ct/R^2ct) \times 100 \quad (2)$$

where R^1_{ct} and R^2_{ct} are the charge transfer resistances in the uninhibited and inhibited solution , respectively. The values of IE% followed the same trend reported for polarization measurements.

3.5. Adsorption isotherm and Mechanism of inhibition

Investigating the adsorption isotherms provide the type of interaction of the tested materials and steel surface. The values surface coverage (θ) were used to determine the adsorption isotherm model by which the adsorption of CSPTA and CSPTA-OA on the steel surface followed. Langmuir adsorption isotherm was found to be the best fit and is given by[47]:

$$C_{(inh)} / \theta = 1/K_{ads} + C_{(inh)} \quad (3)$$

Where $C_{(inh)}$ is inhibitor concentration and Kads is the equilibrium constant for the adsorption process. The Langmuir isotherm was obtained by plotting C/θ vs. C and is shown in Figure 8a and 8b for CSPTA and CSPTA-OA, respectively. A linear relation was obtained in both inhibitors with regression coefficients of 0.999 and 0.998 and slope of 0.997 and 1.02 for CSPTA and CSPTA-OA, respectively. The obtained data suggesting that Langmiur isotherm fit well with the experimental data for both inhibitors. Accordingly, the determined adsorption equilibrium constant obtained from plot of

C/θ vs. C (Equation (3)) can be utilized to determine the standard free energy of adsorption (ΔG^{o}ads) as follows [48-49]:

$$\Delta G^{o} = -RT \ln (55.5Kads) \quad (4)$$

The ΔG^{o} was calculated for CSPTA and CSPTA-OA and found to be -35.49 kJ mol/1and 35.38 kJ mol/1, respectively. The negative value of ΔG^{o}ads indicates the stability and spontaneity of the adsorption process and indicates that the adsorption of CSPTA and CSPTA-OA occurred via physical and chemical adsorption between the CSPTA and CSPTA-OA and the steel surface [50-54].

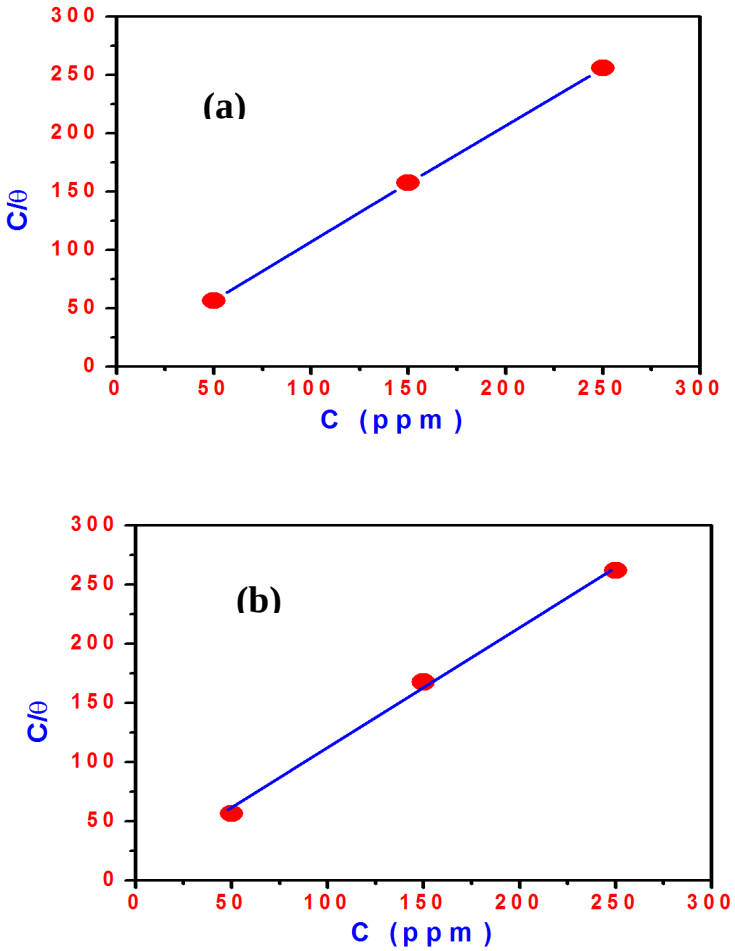

Figure 8. Langmuir adsorption plot of steel in 0.1 M HCl solution containing different concentrations of: (a) CSPTA (b) CSPTA-OA

The corrosion inhibition mechanism of CSPTA and CSPTA-OA in 1 M HCl can be illustrated on the basis of physical and chemical adsorption mechanism on the electrode surface. The inhibition mechanism is based on replacement the interaction between water and steel surface through new interactions with inhibitor molecules as illustrated in Scheme 2. The data of corrosion inhibition indicated that the corrosion inhibition reduced both anodic and cathodic reactions. In this respect, the donor–acceptor interaction between steel ions (Fe^{2+}) and oxygen, nitrogen or double bonds of oleic group enhances the adsorption of CSPTA and CSPTA-OA on the anodic sites. Moreover, the

quaternary amine group exist in CSPTA and CSPTA-OA in the acidic medium gets adsorbed on the cathodic sites, retarding the hydrogen evolution. Accordingly, the unreacted amine groups of CSPTA is protonated in 1 M HCl and consequently, the CSPTA inhibits the corrosion of steel and reduces the cathodic corrosion effectively more than CSPTA-OA due to the presence of lone pair of electrons on nitrogen and positive charge on quaternary ammonium group [55].

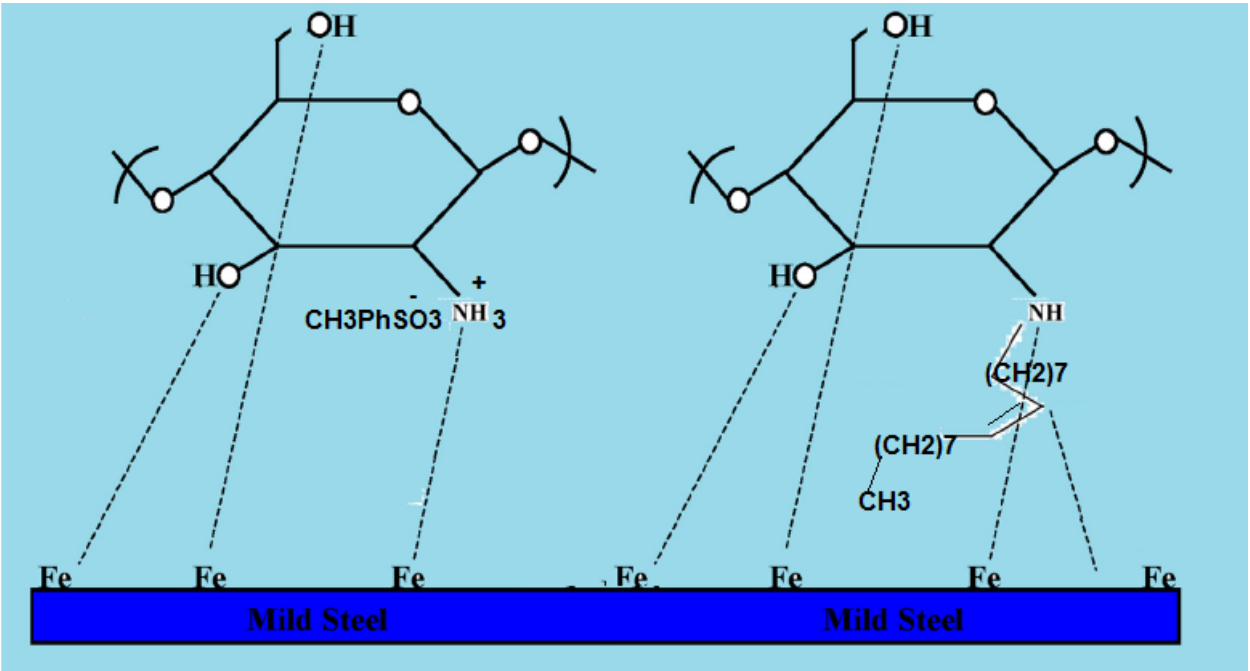

Scheme 2. Adsorption of amphiphile chitosan on the steel surface.

4. CONCLUSIONS

1- Electrochemical data showed that CSPTA and CSPTA-OA have good corrosion protection performance for acid-induced corrosion of steel.
2- Adsorption of the CSPTA and CSPTA-OA on steel surface obeys the Langmuir isotherms.
3. Impedance spectra shows a single capacitive loop and its diameter increases with increasing the CSPTA and CSPTA-OA concentrations.
4. The calculated values of IE from EIS method follow the same trend as those obtained from the polarization results.

ACKNOWLEDGEMENT
The project was financially supported by King Saud University, Vice Deanship of Research Chairs.

References

1. J. Carneiro, J. Tedim, S. C. M. Fernandes, C. S. R. Freire, A. Gandini, M. G. S. Ferreira, M. L. Zheludkevich, *Surf. Coat. Tech.*, 226 (2013) 51–59
2. J. Yuan, C. Giordano, M. Antonietti, *Chem. Mater.*, 22 (2010) 5003–5012.

3. N. V. Likhanova, O. Olivares-Xometl, D. Guzmán-Lucero, Marco A. Domínguez-Aguilar, N. Nava, M. Corrales-Luna, M. C. Mendoza, *Int. J. Electrochem. Sci.,* 6 (2011) 4514 - 4536.
4. V. V. Shevchenko, A. V. Stryutsky, N. S. Klymenko, M. A. Gumenna, A. A. Fomenko,V. N. Bliznyuk, V. V. Trachevsky, V. V. Davydenko, V. V. Tsukruk, *Polymer*, 55 (2014) 3349-3359.
5. E. Kowsaria, M. Payamia, R. Aminib, B. Ramezanzadehb, M. Javanbakhtaa, *Appl. Surf. Sci.,* 289 (2014) 478–486.
6. Y. Sangeethaa, S. Meenakshia, C. S. Sundaramb, *Int. J. Biol. Macromol.,* 72 (2015) 1244–1249.
7. K. M. Manamela, L. C. Murulana, M. M. Kabanda, E. E. Ebenso, *Int. J. Electrochem. Sci.,* 9 (2014) 3029–3046.
8. H. Ashassi-Sorkhabi, M. Es'haghi, *Mater. Chem. Phys.,* 114 (2009) 267–271.
9. Y. C. Wang, T. C. Lee, J. Y. Lin, J. K. Chang, C. M. Tseng, *Corros. Sci.,* 78 (2014) 81–88
10. P. Zhao, C. Zhong, L. Hunag, L. Niu, F. Zhang, *Corros. Sci.,* 50 (2008) 2166–2171.
11. H. Ashassi-Sorkhabi, M. Es'haghi, *Mater. Chem. Phys.,* 114 (2009) 267–271.
12. S. K. Shukla, A. K. Mishra, O. A. Arotiba, B. B. Mamba, *Int. J. Biol. Macromol.,* 59 (2013) 46–58.
13. R. A. A. Muzzarelli, C. Muzzarelli, *Adv. Polym. Sci.,* 186 (2005) 151–209.
14. W. S. C. Paul, *STP Pharma Sci.,* 10 (2000) 5–22.
15. S. Mima, M. Miya, R. Iwamoto, S. Yoshikawa, *J. Appl. Polym. Sci.,* 28 (1983) 1909–1917.
16. G. Crini, *Prog. Polym. Sci.,* 30 (2005) 38–70.
17. F. Ham-Pichavant, G. Sebe, P. Pardon, V. Coma, *Carbohyd. Polym.,* 61 (2005) 259–265.
18. L. T. Ng, S. Swami, *Carbohyd. Polym.,* 60 (2005) 523–528.
19. Z. Yao, C. Zhang, Q. Ping, L. Yu, *Carbohyd. Polym.,* 68 (2007) 781–792
20. A. Safavi, F. Farjami, *Biosens. Bioelectron.,* 26 (2011) 2547–2552.
21. Y. Wu, T. Sasaki, S. Irie, K. A. Sakurai, *Polymer,* 49 (2008) 2321–2327.
22. L. Huang, M. Zhai, J. Peng, L. Xu, J. Li, G. Wei, *Carbohyd. Polym.,* 71 (2008) 690–693.
23. S. S. Keskin, D. D. Kayrak-Talay, U. U. Akman, O. O. Hortacsu, *J. Supercrit. Fluids,* 43 (2007) 150–180.
24. G. A .EL-Mahdy, A. M. Atta, H. A. Al-Lohedan and A.O. Ezzat, *Int. J. Electrochem.Sci*. 4 (2014)7925.
25. I. A. Sogias, V. V. Khutoryanskiy, A. C. Williams, *Macromol. Chem. Phys.,* 211 (2010) 426–433.
26. D. de Britto, L. A. Forato, O. B. G. Assis, *Carbohydr. Polym.,* 74 (2008), 86–91.
27. X. F. Liu, Y. L. Guan, D. Z. Yang, Z. Li, K. D. Yao, *J. Appl. Polym. Sci.,* 79 (2001) 1324–1335.
28. Y. I. Jeong, D. G. Kim, M. K. Jang, J. W. Nah, *Carbohydr. Res.,* 343 (2008) 282–289.
29. R. Belalia, S. Grelier, M. Benaissa, V. Coma, *J. Agric. Food Chem.,* 56 (2008) 1582–1588.
30. C. K. S. Pillai, W. Paul, C. P. Sharma, *Prog. Polym. Sci.,* 34 (2009) 641–678.
31. Y. W. Cho, Y. N. Cho, S. H. Chung, G. Yoo, S. W. Ko, *Biomaterials,* 20 (1999) 2139–2145.
32. Y. Sangeethaa, S. Meenakshia, C. S. Sundaramb, *Int. J. Biol. Macromol.,* 72 (2015) 1244–1249
33. P. C. Schulz, M. S. Rodriguez, L. F. Del Blanco, M. Pistonesi, E. Agull, *Colloid Polym. Sci.,* 276 (1998) 1159–1165.
34. I. Pepić, J. Filipović-Grčić , I. Jalšenjak , *Colloid Surface A,* 327 (2008) 95–102.
35. M. A. Quraishi, A. Singh, V. Singh, D. Yadav, A. K. Singh, *Mater. Chem. Phys*. 122 (2010)114–122.
36. O. L. Riggs, Corrosion Inhibitors, 2nd ed.; C. C. Nathan: Houston, TX, USA, 1973; p 109.
37. Q. Qu, Z. Hao, L. Li, W. Bai, Z. Ding, *Corros. Sci.,* 51 (2009) 569–574.
38. F. Bentiss, M. Lebrini, M. Lagrenée, *Corros. Sci.,* 47 (2005) 2915–2931.
39. Q. Qu, S. Jiang, W. Bai, L. Li, *Electrochim. Acta,* 52 (2007) 6811–5820.
40. R. Solmaz. *Corros. Sci.,* 81 (2014) 75–84.
41. M. S. Morad, *Corros. Sci.,* 42 (2000) 1307–1326.
42. M. Lebrini, F. Bentiss, N. Chihib, C. Jama, J. P. Hornez, M. Lagrenée, *Corros. Sci.,* 50 (2008) 2914–2918.

43. B. S. Sanatkumar, J. Nayak, *Int. J. Hydrogen Energ.*, 37 (2012) 9431–9442.
44. S. Rames, S. Rajeswari, *Electrochim. Acta* 49 (2004) 811–820.
45. E. Chaieb, A. Bouyanzer, B. Hammouti, M. Benkaddour, *Appl. Surf. Sci.* 246 (2005) 199–206.
46. A. Dadgarnezhad, I. Sheikhshoaie, F. Baghaei, *Anti-Corros. Meth. Mater*. 51 (2004) 266–271.
47. M. Lebrini, F. Bentiss, H. Vezin, M. Lagrenee, *Corros. Sci.*, 48 (2006) 1279–1291
48. C. M. Goulart, A. Esteves-Souza, C. A. Martinez-Huitle, C. J. F. Rodrigues, M. A. M. Maciel, A. Echevarria, *Corros. Sci.*, 67 (2013) 281–291.
49. H. Keles, M. Keles, I. Dehri, O. Serindag, *Mater. Chem. Phys.*, 112 (2008) 173–179.
50. E. Bayol, A. A. Gurten, M. Dursun, K. Kayakırılmaz, *Acta Phys. – Chim. Sin.*, 24 (2008) 2236–2242.
51. G. Avc, *Mater. Chem. Phys.*, 112 (2008) 234–238.
52. M. Lebrini, F. Robert, H. Vezin, C. Roos, *Corros. Sci.*, 52 (2010) 3367–3376.
53. M. J. Bahrami, S. M. A. Hosseini, P. Pilvar, *Corros. Sci.*, 52 (2010) 2793–2803.
54. E. A. Noor, A. H. Al-Moubaraki, *Mater. Chem. Phys.*, 110 (2008) 145–154.
55. Y. Sangeethaa, S. Meenakshia, C. S. Sundaramb, Int. J. Biol. Macromol. 72 (2015) 1244–1249.